Bending Stiffness Depends on Curvature of Ternary Lipid Mixture Tubular Membranes

Aiwei Tian,[†‡] Benjamin R. Capraro,[†] Cinzia Esposito,[†] and Tobias Baumgart[†‡*]
[†]Department of Chemistry and [‡]Department of Chemical and Biomolecular Engineering, University of Pennsylvania, Philadelphia, Pennsylvania

ABSTRACT   Lipid and protein sorting and trafficking in intracellular pathways maintain cellular function and contribute to organelle homeostasis. Biophysical aspects of membrane shape coupled to sorting have recently received increasing attention. Here we determine membrane tube bending stiffness through measurements of tube radii, and demonstrate that the stiffness of ternary lipid mixtures depends on membrane curvature for a large range of lipid compositions. This observation indicates amplification by curvature of cooperative lipid demixing. We show that curvature-induced demixing increases upon approaching the critical region of a ternary lipid mixture, with qualitative differences along two roughly orthogonal compositional trajectories. Adapting a thermodynamic theory earlier developed by M. Kozlov, we derive an expression that shows the renormalized bending stiffness of an amphiphile mixture membrane tube in contact with a flat reservoir to be a quadratic function of curvature. In this analytical model, the degree of sorting is determined by the ratio of two thermodynamic derivatives. These derivatives are individually interpreted as a driving force and a resistance to curvature sorting. We experimentally show this ratio to vary with composition, and compare the model to sorting by spontaneous curvature. Our results are likely to be relevant to the molecular sorting of membrane components in vivo.

INTRODUCTION

Motivated by the aim to understand how molecular sorting of membrane components is achieved in biological cells (1,2), the coupling between membrane curvature and composition has recently been under intensive investigation. In addition to proteins, fluorescent lipids have been used as trafficking markers. Importantly, lipidlike dyes of the indocarbocyanine family with identical headgroups were shown to display remarkably different sorting in cells (3). The protein cholera toxin subunit B is, furthermore, frequently used to study intracellular trafficking (4). We demonstrated that these lipidlike fluorophores with differing intrinsic curvature were not significantly sorted in membranes with steep curvature gradients (5). Conversely, we found that cholera toxin subunit B is effectively sorted among connected membranes with differing curvature (5).

Several different types of membrane curvature can be distinguished in cells (6,7). Among these, membranes with spherical (e.g., vesicles) and cylindrical curvature (e.g., membrane tubes) are the most prominent long-lived high curvature intracellular membrane morphologies. Our research focuses on biophysical characterization of sorting in tubular membranes. Biological membrane tubes have recently received increasing interest in various contexts, including intercellular nanotubes with signaling function (8) and intracellular tubes connecting different organelles (9).

For a quantitative characterization of mechanical contributions to the sorting of membrane components, lipid model membrane systems have proved advantageous. Evidence

for the sorting of fluid phase domains with differing bending stiffness came from fluorescence microscopy images of giant unilamellar vesicles with liquid-ordered (L_o) and liquid-disordered (L_d) phase coexistence (10,11). Lateral segregation has also been observed in tubular model membranes (10,12). Lipid bilayer membrane tubes have long been of interest to biophysicists (13–15), and model membrane tubes with complex composition are receiving increasing attention (5,12,16–18). This contribution investigates how curvature sorting is amplified in nonideally mixing multicomponent membranes.

The coupling between membrane curvature and composition has been theoretically investigated. Several continuum theories have been developed. An early analytical exposition is the one by Markin (19), who proposed the composition dependence of the models of spontaneous curvature and bending stiffness considered in this work. Kozlov developed a thorough thermodynamic analysis of elastic amphiphile mixture interfaces (20,21), which forms the basis of the analytical component of this contribution. Phenomenological continuum theories predicted curvature instabilities (22,23) and curvature-induced phase segregation in vesicles (24), and several, more recent contributions have computed membrane composition profiles as a function of curvature (25–27). In the strong segregation limit, the influence of elastic domain properties on membrane shape has been investigated (28–35) and the weak segregation limit has also been explored (22,23,36). Dynamic aspects associated with curvature-composition coupling and phase transitions influenced by membrane proteins have recently been investigated (37). Most of these studies focused on the role of local spontaneous curvature, as opposed to bending stiffness,

---

in coupling membrane shape and composition. Several previous experimental studies have examined the effect of composition on bending stiffness. Amphiphilic membranes of interest have included emulsions (38,39) and lipid bilayers (12,40–42).

MATERIALS AND METHODS

Materials

1,2-dioleoyl-*sn*-glycero-3-phosphocholine (DOPC), cholesterol (Chol), 1,2-dipalmitoyl-*sn*-glycero-3-phosphocholine (DPPC), 1-stearoyl-2oleoyl-*sn*-glycero-3-phosphocholine (SOPC), and distearoylphosphatidyl-ethanolamine-*N*-[biotinyl(polyethylene glycol)2000] (DSPE-Bio-PEG2000) were from Avanti Polar Lipids (Alabaster, AL). Fatty-acid free bovine serum albumin was obtained from Sigma Chemical (St. Louis, MO). Texas Red-1,2-dihexadecanoyl-*sn*-glycero-3-phosphoethanolamine triethylammonium salt (TR-DHPE) was purchased from Invitrogen (Carlsbad, CA).

Vesicle preparation, micropipette fabrication, and tether pulling method were as previously described (5) (also see Supporting Material).

Membrane tension, tether radius, and bending stiffness determination

Lateral membrane tension σ is obtained from pipette aspiration pressure ΔP, by the formula (43)

$$\sigma = \Delta P \frac{R_p}{2\left(1 - R_p/R_v\right)}, \qquad (1)$$

in which R_p and R_v are the pipette radius and vesicle radius (of the spherical part of the vesicle outside of the pipette; also see Supporting Material), respectively.

Membrane tension determines a corresponding tether radius. The tether radius is obtained from stepwise horizontal elongation and release of the membrane tube as described in Tian and Baumgart (5). Briefly, the tether was typically elongated in three-to-five steps (each of 20 μm) and the associated change in the length of the pipette-aspirated vesicle projection was measured. The tether radius can then be calculated from the ratio of projection length change (ΔL_p) and tether length change (ΔL_t). The ratios (i.e., the slopes) at different membrane tensions are shown later in Fig. 2 *a*.

From the conservation of membrane area and total vesicle volume, the following relation can be obtained, which we used to calculate tether radii (44,45):

$$R_t = -\frac{\Delta L_p}{\Delta L_t}\left(1 - \frac{R_p}{R_v}\right)R_p. \qquad (2)$$

The influence on the determination of R_t of vesicles with prolate spheroid shape is quantitatively discussed in the Supporting Material. Briefly, the error is negligible under all conditions used.

Imaging

Vesicles were imaged by fluorescence confocal microscopy scanning system (model No. FV300 integrated with a motorized inverted microscope IX81; Olympus, Center Valley, PA), using a 60×, 1.2 NA water immersion lens with coverslip correction collar (Olympus). Illumination intensities and illumination times were minimized to reduce photoeffects (46). Image analysis was performed using IMAGEJ (National Institutes of Health, Bethesda, MD).

Additional methods (error propagation analysis and method of bending stiffness determination by micropipette aspiration) are described in the Supporting Material.

RESULTS

We focused our investigation of curvature-dependent sorting on the ternary lipid mixture DOPC, DPPC, and Chol, the phase behavior of which is well characterized (47,48) (see Fig. 1). We chose six different compositions (labeled I–VI in Fig. 1) made with these three lipid types. Vesicles were prepared with the addition of the fluorophore TR-DHPE, as well as a biotinylated lipid with oligo-ethyleneglycol spacer, which allowed us to couple streptavidin-coated beads to the vesicular membranes. The large majority of vesicles prepared with these six compositions were optically homogenous as determined by fluorescence microscopy, in accordance with the published phase diagram (47,48). To localize the position of the phase boundary and critical point at our measurement temperature (22 $\pm$ 0.5°C) in the ternary phase diagram, we determined approximate area fractions as well as the fraction of phase-separated vesicles. The resulting phase boundary shown in Fig. 1 is in good agreement with data by Veatch and Keller (47). Only optically homogenous vesicles were examined in the experiments below. We selected two different compositional trajectories: one approximately parallel to the phase boundary (compositions I–III), and one roughly orthogonal to the phase boundary (compositions III–VI); see Fig. 1. These two compositional directions are expected to lead to differing critical exponents of thermodynamic quantities (49). According to the phase
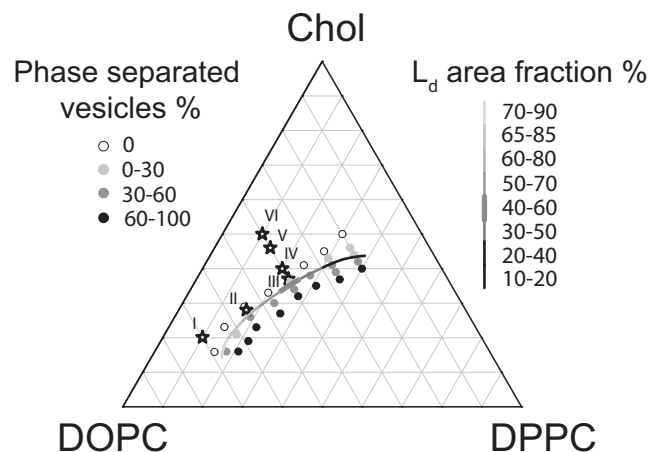

FIGURE 1 Experimental phase diagram indicating compositions (depicted using *stars*) of ternary lipid mixture DOPC/Chol/DPPC: I, 70:20:10; II, 55:28:17; III, 40:37:23; IV, 40:40:20; V, 40:46:14; and VI, 40:50:10. Circles mark compositions of vesicles imaged to determine the upper phase boundary and the critical point of phase separation (critical consolute point). Population fractions of vesicles with phase separation are indicated in the left legend. The grayscale line represents the upper phase boundary binodal line at ~22°C. The binodal line also displays the area fractions of the disordered phase according to the legend on the right. Compositions III and IV are in the neighborhood of the critical point where area fraction is 40–60% (indicated by the *thick bar* on *binodal* and *right legend*). Our compositions I–VI are chosen in the homogeneous phase region outside the miscibility gap and approach the neighborhood of the critical point in two directions: along lines parallel (I, II, and III) and lines perpendicular (VI, V, IV, and III) to the upper phase boundary.
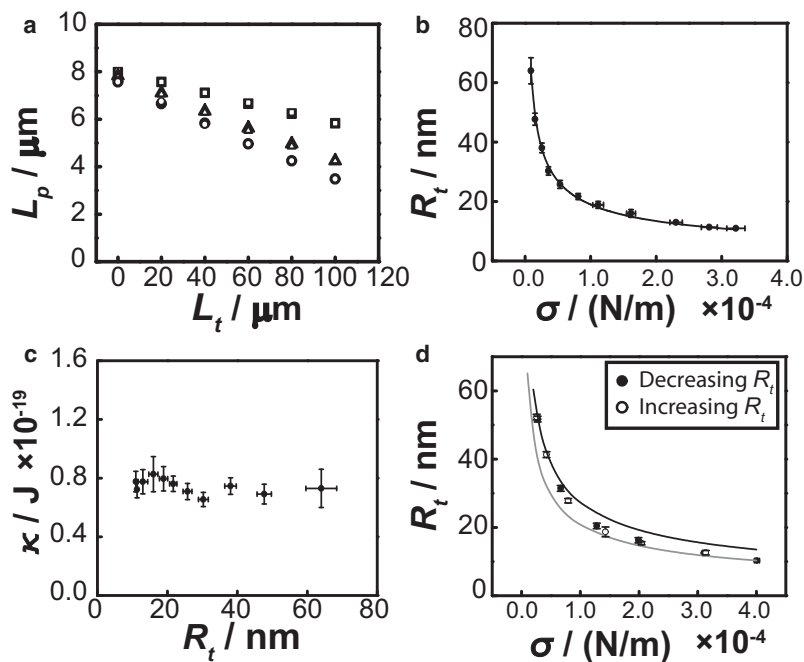
FIGURE 2 Membrane bending stiffness from projection length (L_p)/tether length (L_t) measurements. (*a*) Demonstration of L_p versus L_t plots at different membrane tensions. (*Square*, $\sigma = 1.2 \times 10^{-4}$ N/m; *triangle*, $\sigma = 5.2 \times 10^{-5}$ N/m; *circle*, $\sigma = 3.4 \times 10^{-5}$ N/m; and *solid* and *open* symbols represent the elongation and relaxation steps of the tether, respectively.) This example is chosen from three tether radius measurements of composition III. From the slopes of these plots, we obtained tether radii (see Eq. 2). (*Square*, $R_t = 20.6$ nm; *triangle*, $R_t = 34.0$ nm; and *circle*, $R_t = 39.0$ nm.) (*b*) Relation of tether radius and membrane tension of a tether consisting of binary mixture DOPC/Chol = 2:1. Solid line indicates the fit of data points using a single bending stiffness ($\kappa = 7.4 \times 10^{-20}$ J). (*c*) Bending stiffness versus tether radius plot. Bending stiffness is calculated from panel *b* and is observed to be roughly constant, under changing curvature. (*d*) Relation of tether radius and membrane tension of a tether from ternary mixture III. Solid and open circles represent decreasing and increasing R_t, respectively. Solid line and shaded line are plots at the maximum ($\kappa_{max} = 1.5 \times 10^{-19}$ J) and the minimum ($\kappa_{min} = 8.5 \times 10^{-20}$ J) bending stiffness values among these data points. It is thus observed that the bending stiffness decreases with curvature for this mixture. Error bars were determined as explained in the Supporting Material.

diagram, compositions III and IV are expected at room temperature to be in the neighborhood of a critical consolute (i.e., mixing/demixing) point (47,48).

Vesicles were pipette-aspirated and the lateral membrane tension was adjusted by a hydrostatic approach, as described in Tian and Baumgart (5). Our approach to determining membrane bending stiffness as a function of curvature is identical to our previous measurements (5), and a similar technique has been described by Bo and Waugh (14). Vesicles with sufficient excess membrane area (relative to the area of a sphere with the same volume) were chosen for pipette aspiration. The excess area yields a pipette-aspirated membrane fraction with a length that should exceed the inner aspiration pipette radius under all experimental conditions. After pipette aspiration, a streptavidin-coated bead was brought into contact with the vesicular membrane by means of a second pipette that was moved via a micromanipulator assembly. Moving the bead away from the vesicle generated a cylindrical tether from the vesicular membrane. The curvature of the tether was adjusted by means of the pipette aspiration pressure. We determined the radius by a stepwise extension of the tube length (L_t) and measurement of the accompanying decrease of the length (L_p) of the pipette-aspirated vesicle projection in the pipette interior (5,14). Examples for such measurements are shown in Fig. 2 *a* for three different lateral membrane tensions. From the slope of the plot in Fig. 2 *a*, the tube radius can be calculated. Examples are shown in Fig. 2 *b*, where, to contrast with ternary mixtures, we consider a binary mixture of DOPC/Chol in a molar ratio 2:1. The line in Fig. 2 *b* is a fit to the equation $R_t = \sqrt{\kappa/2\sigma}$ (50,51). The excellent agreement between fit and experimental data in Fig. 2 *b* indicates that the binary

mixture membrane displays a constant bending stiffness over the entire curvature range, down to ~10 nm. This finding is further demonstrated in the bending stiffness values that were calculated from every radius/tension pair, shown in Fig. 2 *c* over the entire curvature range. Earlier measurements using binary mixtures of palmitoyloleoyl-phosphatidylserine and SOPC also did not report a curvature-dependent bending stiffness (52).

Fig. 2 *d* shows radius measurement examples in a tube with composition III (close to the critical point). The lines in Fig. 2 *d* are tube radius values calculated for a constant bending stiffness assuming either the stiffness value (κ_{max}) obtained from the radius/tension pair of the largest radius in Fig. 2 *d* (*solid line*), or the stiffness value (κ_{min}) obtained from the radius/tension pair of the smallest radius value (*shaded line*). Clearly, the experimental data cannot be fitted by assuming a constant bending stiffness. In Fig. 3, we illustrate the bending stiffness values obtained from the radius/tension pairs shown in Fig. 2 *d* for composition III in three different representations: as a function of tube radius (Fig. 3 *a*); as a function of curvature, $C = 1/R_t$, where R_t is the tube radius (Fig. 3 *b*); and, as a function of the square of the tube curvature (Fig. 3 *c*). Fig. 3 *c* indicates a different slope for the first few data points, compared to those obtained at larger curvatures. The axis scaling of Fig. 3 *c* is motivated by an analytical theory (detailed below), which will indicate the bending stiffness to be a function of the squared curvature in the low curvature regime. Fig. 3 *d* displays data collected for measurements in eight different vesicles over the entire curvature range of composition III.

Before we quantitatively examine our data (results shown in Fig. 4), we outline the theoretical framework of our
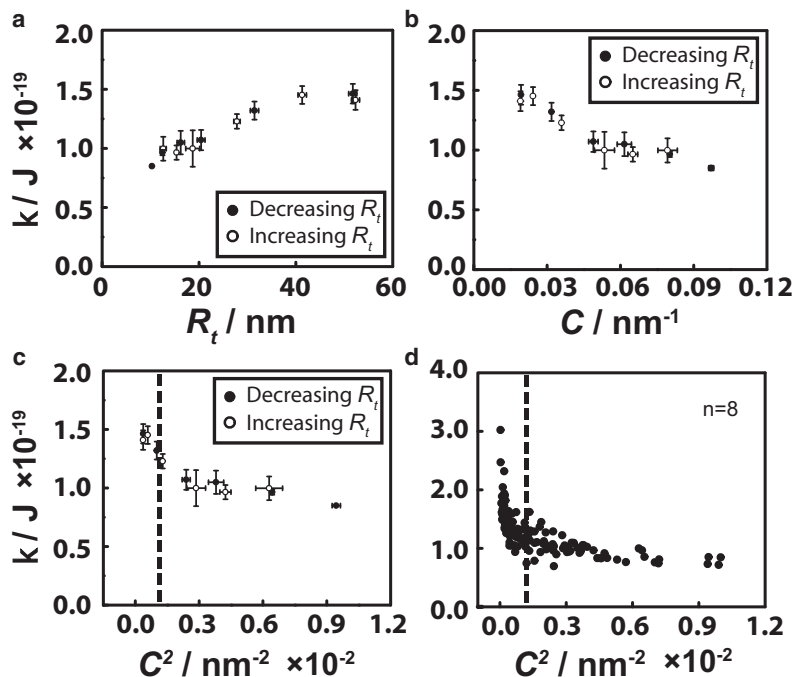
FIGURE 3 Bending stiffness versus (a) tether radius, (b) tether curvature, and (c) squared curvature plots from the same experimental data shown in Fig. 2 d. The figures clearly indicate the bending stiffness to decrease with increasing curvature. (d) Bending stiffness and squared curvature C^2 relation from combination of eight whole-range data sets of composition III. The value n refers to the number of different vesicles examined. Data points in panels c and d are separated into two ranges by dashed lines at $C^2 = 0.0012$ nm^{-2}. The bending stiffnesses obtained at C^2 values <0.0012 nm^{-2} were chosen for fitting our thermodynamic model to bending stiffness-curvature relations $\kappa_{\text{eff}} = \kappa_0 - \Omega C^2$, for all compositions examined.

analysis and contrast description of sorting caused by composition-dependent spontaneous curvature (19,21,22, 24,27) to sorting invoked by composition-dependent bending stiffness in membrane mixtures. To apply the theory developed by Kozlov and Helfrich (21) to our situation, we first approximate the ternary mixture of Fig. 1 with a binary mixture. Previous work has shown that a quasibinary

phenomenological condensed complex model well describes the fluid phase boundaries of experimental ternary phase diagrams (53). Below, we obtain alternative expressions for ternary mixtures. These expressions are more complex but do not change the interpretation of experimental data. We consider a thermodynamic process that keeps the area of the membrane tube constant but changes the
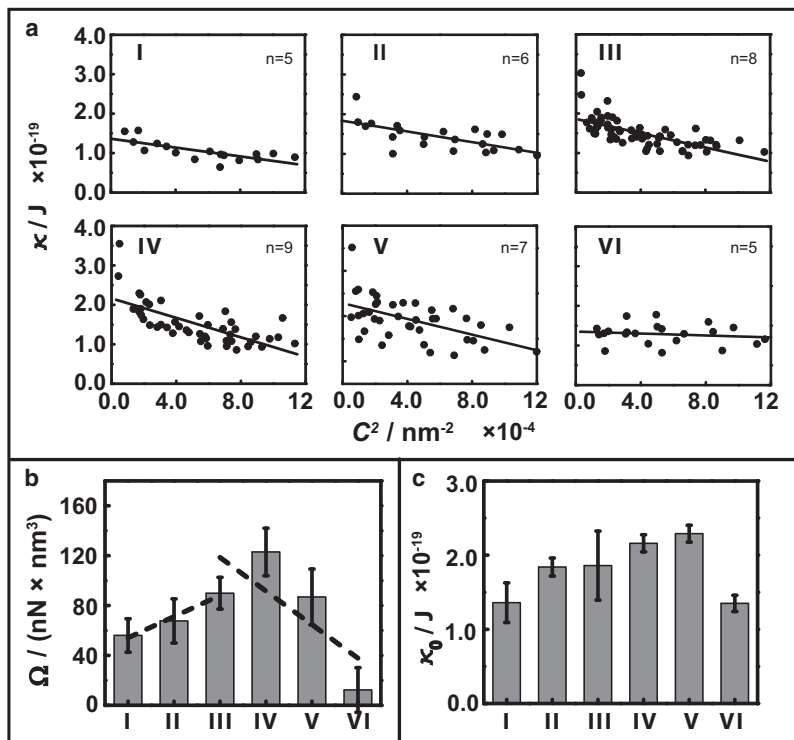

FIGURE 4 (a) Linear fits of bending stiffness and squared curvature obtained from multiple data sets in the low curvature range ($C^2 < 0.0012$ nm^{-2}) for each composition. Compositions are indicated at the upper-left corner of each graph, and the numbers of tethers included for each composition are shown in the upper-right corner of each plot. Data sets of composition III are the same as those in Fig. 3 d but display the low curvature region instead of the whole range. (b) Slopes from linear fits for different compositions in panel a. Dashed lines are linear fits depicting the increasing trends of slopes Ω for compositional trajectories parallel (I, II, and III) and perpendicular (VI, V, IV, and III) to phase boundary approaching the neighborhood of a critical demixing point. The graph indicates that the slope Ω, which determines the sorting efficiency (see Eqs. 7 and 8), increases upon approaching the critical region. (c) Bending stiffness at zero curvature (intercepts of plots in panel a) for different compositions. Error bars in panels b and c are the uncertainty of linear fits in panel a.

curvature (compare to the Appendix of Kozlov and Helfrich (21)) and thus define the differential of the tube free energy, F, as

$$dF = A\kappa C dC + \mu_\alpha dN_\alpha + \mu_\beta dN_\beta$$
$$= A\kappa C dC + N(\mu_\alpha - \mu_\beta)d\varphi_\alpha, \tag{3}$$

where A is the tube area, κ is the bending stiffness of the tube, and μ_i and N_i are chemical potentials and numbers of molecular components i, respectively. Expansions with respect to mole fraction φ_i (as opposed to molecular component numbers N_i) simplify the resulting expressions. Equation 3 allows us to obtain a Taylor expansion of the tube free energy (21) about a flat membrane from expansions of the intensive parameters in Eq. 3, followed by integration (see Appendix of Kozlov and Helfrich (21)). We define the diffusion (or exchange) potential as

$$\overline{\mu} = \mu_\alpha - \mu_\beta = \frac{1}{N}\left(\frac{\partial F}{\partial \varphi_\alpha}\right)_{A,C}, \tag{4}$$

where N is the total number of molecules in the tube, and the derivative is evaluated at constant tube area and constant curvature. All following derivatives are evaluated at constant area; however, below we drop the index A. As Appendix A demonstrates in more detail, an expansion of the quantity $\overline{\mu}$ to first-order in curvature and composition change relative to zero curvature,

$$\Delta\varphi_\alpha = \varphi_\alpha(C) - \varphi_{\alpha 0},$$

yields the following relation between these two quantities,

$$\Delta\varphi_\alpha = -\left\{\left(\frac{\partial \overline{\mu}}{\partial C}\right)_0 \bigg/ \left(\frac{\partial \overline{\mu}}{\partial \varphi_\alpha}\right)_0\right\}C, \tag{5}$$

from which an effective bending stiffness can be obtained (see Appendix A),

$$\kappa_{\text{eff}} = \kappa_0 - \rho\left(\frac{\partial \overline{\mu}}{\partial C}\right)_0^2 \bigg/ \left(\frac{\partial \overline{\mu}}{\partial \varphi_\alpha}\right)_0, \tag{6}$$

where $\rho = N/A$ is an area density that is assumed to be constant. The index 0 in Eqs. 5 and 6 indicates that these partial derivatives have to be evaluated for the flat membrane, as they are Taylor coefficients associated with an expansion about the flat state of the membrane. Note that under our experimental conditions the curvature of the vesicle is 2–3 orders-of-magnitude smaller compared to the curvature of the tube. We therefore regard the vesicle as flat. Furthermore, the number of lipids contained in the vesicle is significantly larger than that in the tube. The vesicle is therefore regarded as a particle reservoir with fixed composition and curvature, and therefore has constant chemical potential. Note that the effective bending stiffness obtained through Eq. 6 is smaller compared to the bare bending stiffness, but is not a function of curvature. Furthermore, the first derivative in Eq. 6 will have nonzero values only for membranes with nonzero spontaneous curvature (see Appendix A, which also provides an example of a model for which the thermodynamic derivatives can be evaluated analytically). For both of these reasons, our observations shown in Figs. 3 and 4 cannot be explained by means of a model that assumes primarily spontaneous curvature to drive the sorting process.

It follows that to obtain a curvature-dependent bending stiffness, the quantity $\overline{\mu}$ has to be expanded to second-order (or, equivalently, the free energy has to be expanded to third-order). From such an expansion, we obtain the composition change as a quadratic function of curvature (see Appendix B for details),

$$\Delta\varphi_\alpha = -\frac{1}{2}\left\{\left(\frac{\partial^2 \overline{\mu}}{\partial C^2}\right)_0 \bigg/ \left(\frac{\partial \overline{\mu}}{\partial \varphi_\alpha}\right)_0\right\}C^2, \tag{7}$$

allowing us to express the bending stiffness as a function of curvature (see Appendix B),

$$\kappa_{\text{eff}} = \kappa_0 - \frac{3}{4}\left\{\left(\frac{\partial \kappa}{\partial \varphi_\alpha}\right)_0^2 \bigg/ \rho\left(\frac{\partial \overline{\mu}}{\partial \varphi_\alpha}\right)_0\right\}C^2 = \kappa_0 - \Omega C^2. \tag{8}$$

Equation 8 is valid at constant chemical potentials fixed by the reservoir. As long as the bending stiffness is composition-dependent, we therefore find the renormalized (effective) bending stiffness to be a quadratic function of curvature. The effective bending resistance is experimentally obtained from

$$\kappa_{\text{eff}} = 2\sigma R_t^2,$$

where σ and R_t are the experimentally determined quantities. Equation 8 is the central result of our analysis and is fitted to data in the form

$$\kappa_{\text{eff}} = \kappa_0 - \Omega C^2,$$

where Ω comprises the thermodynamic derivatives in Eq. 8. Note that these derivatives are approximately constant for given initial conditions, as they are all evaluated at the flat state.

In both Eqs. 6 and 8, the effective bending stiffness depends on a quantity that can be interpreted as a "driving force" to sorting (the first derivative in both equations). This "driving force" is divided by a quantity that resists sorting (second derivative in both equations). The resistance to sorting is composition-dependent (see Appendix B for details including a model for which the thermodynamic derivatives were analytically evaluated). For membranes that can phase-separate, this derivative will vanish at the spinodal line, in the neighborhood of which sorting is thus expected to be amplified. The spinodal line, which lies within the miscibility gap of the phase diagram, can be approached most closely in the neighborhood of a critical point. This motivates our choice of compositional trajectories (Fig. 1). We fitted Eq. 8 to our data within the low curvature regime defined in Fig. 3. The

rationale behind this limited range evolves from the derivation of Eq. 8. The relation results from Taylor expansions about the flat state. The second-order Taylor expansion of tube free energy in curvature has been shown to be accurate down to curvature radii approaching membrane thickness (54). However, it is likely that the accuracy of a second-order free energy expansion (first-order expansion of the chemical potentials) in composition change is limited to small deviations from the composition of the flat membrane for the mixing ratios considered in this contribution.

Fig. 4 summarizes our composition-dependent measurements of bending stiffness for the six compositions of Fig. 1. Fig. 4 a shows the low curvature regime of bending stiffness versus squared curvature plots that, according to Eq. 8, is expected to be linear. Results of linear fits to data obtained from several vesicles (numbers n are indicated in the figure) are displayed in Fig. 4, b and c. The error bars in Fig. 4, b and c, result from the uncertainty of slope and intercept of linear fits to the pooled data shown in Fig. 4 a. Although these error bars are large, Fig. 4 b suggests that the prefactor Ω increases upon approaching the neighborhood of the critical point along the trajectory roughly parallel to the phase boundary (compositions I–III). As further discussed below, this may be rationalized by the value of the second derivative in Eq. 8 becoming smaller along this trajectory. We furthermore observe that approaching the critical region along the trajectory orthogonal to the phase boundary is also associated with an increase of the prefactor Ω. Refined measurements will have to be performed to determine critical exponents in these experiments, because the current uncertainties are large. Our results, however, do indicate that effective sorting, indicated by composition-dependent bending stiffness values, occurs over a large composition range far from the critical point.

Fig. 4 c displays bending stiffness values for the flat state obtained from fitting Eq. 8 to our data. The figure indicates that the reservoir bending stiffness κ_0 increases when approaching the critical neighborhood through compositions I–III. Bending stiffness measurements in ternary mixture membranes are still rare (55,56). We therefore used a second technique to confirm the composition dependence of the bending stiffness of the vesicle reservoir displayed in Fig. 4 c. We measured projected membrane area of aspirated vesicles as a function of lateral tension, and determined bending stiffness (57) as described in the Supporting Material. We minimized curvature effects in these measurements by using large pipettes and focusing on the low tension regime. We first confirmed (see Table 1) that our experi-

TABLE 1 Bending stiffness of quasiflat membranes by pipette aspiration and tether pulling

Composition	$\kappa_0 \times 10^{-19}$ J (Aspiration)	$\kappa_0 \times 10^{-19}$ J (Tether)
I	0.91 ± 0.17 ($n = 4$)	1.36 ± 0.27 ($n = 5$)
II	—	1.84 ± 0.12 ($n = 6$)
III	—	1.86 ± 0.47 ($n = 8$)
IV	1.40 ± 0.52 ($n = 8$)	2.16 ± 0.12 ($n = 9$)
V	—	2.29 ± 0.11 ($n = 7$)
VI	0.93 ± 0.13 ($n = 4$)	1.36 ± 0.11 ($n = 5$)
DOPC/Chol = 1:1	0.91 ± 0.33 ($n = 10$)	—
DOPC/Chol = 2:1	0.86 ± 0.13 ($n = 8$)	1.01 ± 0.23 ($n = 9$)
SOPC	0.77 ± 0.14 ($n = 13$)	—

Comparison of experimental bending stiffness values using micropipette aspiration method and tether pulling, respectively. Uncertainties result from measurements in n vesicles indicated in parentheses.

mental conditions reproduced bending stiffness values for the lipid SOPC, which has frequently been used in pipette aspiration experiments (57,58). Previous measurements have shown that bending stiffness often increases while increasing the cholesterol content of fluid phase binary mixture membranes (40,41). However, interestingly, cholesterol has a surprisingly small effect on the bending stiffness of binary mixtures with DOPC (42). This phenomenon is confirmed by our pipette aspiration measurements (Table 1). Overall, the stiffness values shown in Table 1 are systematically smaller, comparing pipette aspiration to membrane tethers. This effect has previously been noted (59) and is likely related to the convolution of bending and stretching elasticities complicating analysis of pipette aspiration data (60). The table does, however, indicate that pipette aspiration reports a similar composition trend of reservoir bending stiffness values compared to values obtained from fitting our Eq. 8. We finally note that our DOPC/Chol bending stiffness values are in good agreement with literature values (42,59).

DISCUSSION

We have thus far interpreted our measurements by means of quasibinary mixture models with straightforward interpretation and minimized algebraic effort. In reality, however, both bending stiffness and chemical potentials depend on the concentrations of all three components—DOPC, DPPC, and Chol. The ternary mixture equivalents to Eqs. 6 and 8 are obtained from an exercise in matrix algebra, using the two exchange potentials $\overline{\mu}_i = \mu_i - \mu_3$ referenced to the chemical potential of the third component. For the effective resistance to bending in the ternary spontaneous curvature model, we have

$$\kappa_{\text{eff}} = \kappa_0 - \rho \frac{\left(\frac{\partial \overline{\mu}_1}{\partial C}\right)_0^2 \left(\frac{\partial \overline{\mu}_2}{\partial \varphi_2}\right)_0 - \left(\frac{\partial \overline{\mu}_1}{\partial C}\right)_0^2 \left(\frac{\partial \overline{\mu}_2}{\partial C}\right)_0 \left(\frac{\partial \overline{\mu}_1}{\partial \varphi_2}\right)_0 + \left(\frac{\partial \overline{\mu}_2}{\partial C}\right)_0^2 \left(\frac{\partial \overline{\mu}_1}{\partial \varphi_1}\right)_0}{\left(\frac{\partial \overline{\mu}_1}{\partial \varphi_1}\right)_0 \left(\frac{\partial \overline{\mu}_2}{\partial \varphi_2}\right)_0 - \left(\frac{\partial \overline{\mu}_1}{\partial \varphi_2}\right)_0 \left(\frac{\partial \overline{\mu}_2}{\partial \varphi_1}\right)_0}, \tag{9}$$

i.e., the sole difference between Eqs. 6 and 8 is the interpretation of the thermodynamic factor. Equivalently, the curvature- and composition-dependent resistance to bending described by Eq. 8 reads, for a ternary mixture,

$$\kappa_{\text{eff}} = \kappa_0 - \frac{3}{4} \frac{\left(\frac{\partial \kappa}{\partial \varphi_1}\right)_0^2 \left(\frac{\partial \overline{\mu}_2}{\partial \varphi_2}\right)_0 - \left(\frac{\partial \kappa}{\partial \varphi_1}\right)_0^2 \left(\frac{\partial \kappa}{\partial \varphi_2}\right)_0 \left(\frac{\partial \overline{\mu}_1}{\partial \varphi_2}\right)_0 + \left(\frac{\partial \kappa}{\partial \varphi_2}\right)_0^2 \left(\frac{\partial \overline{\mu}_1}{\partial \varphi_1}\right)_0}{\rho \left\{ \left(\frac{\partial \overline{\mu}_1}{\partial \varphi_1}\right)_0 \left(\frac{\partial \overline{\mu}_2}{\partial \varphi_2}\right)_0 - \left(\frac{\partial \overline{\mu}_1}{\partial \varphi_2}\right)_0 \left(\frac{\partial \overline{\mu}_2}{\partial \varphi_1}\right)_0 \right\}} C^2, \tag{10}$$

where the ratio of thermodynamic derivatives is the ternary version of the parameter Ω determined from the fits shown in Fig. 4. Presently, little is known about composition dependence of κ and $\overline{\mu}_i$ along lines parallel to the edges of the Gibbs phase triangle representing ternary mixtures. Future experimental measurements of ternary mixture bending stiffness values across the phase diagram will, we hope, allow to test the detailed form of Ω.

We have approached the critical mixing/demixing region of a ternary lipid mixture from two different compositional directions, one approximately orthogonal and one roughly parallel to the phase boundary. Comparing these two trajectories, Fig. 4 suggests that along the direction orthogonal to the phase boundary the parameter Ω decreases more quickly away from the critical point compared to the trajectory asymptotically parallel to the phase boundary. It is a well-known fact that critical exponents associated with the liquid/gas phase transition in a single component system differ, comparing the approach of the critical point asymptotically parallel versus along a direction orthogonal to the coexistence curve in field space (49). The scaling behavior of mixtures satisfies the same scaling laws as single component systems, if suitable field variables are introduced (61,62), alternative to the densities (mole fractions) of Fig. 1. A more trivial challenge to the measurement of critical exponents is the large uncertainty in our present measurements.

Bending stiffness values κ_0 of the quasiflat reservoir were observed to increase when approaching the phase boundary along the trajectory of compositions I–III (Fig. 4 c and Table 1), i.e., along a trajectory with increasing DPPC concentration. Importantly, this behavior in approaching a demixing transition phase boundary is opposite to the trends in bending stiffness near a main phase transition in single component membranes. In DMPC membranes, for example, a significant softening occurs when decreasing temperature toward the phase transition temperature (63–65). This decreased bending stiffness is likely due to a divergence of the area compressibility modulus at the DMPC main phase transition temperature (59,66). On the other hand, the area compressibility modulus of ternary lipid mixtures does not appear to show anomalies near a mixing/demixing phase boundary (56). In the critical neighborhood of a mixing/demixing tran-

sition in ternary mixtures, the area compressibility modulus and bending stiffness thus appear to remain finite, whereas the osmotic compressibility diverges. We therefore argue that the increase of the quantity Ω, defined in Eq. 8, upon approaching the critical neighborhood, is dominated by the divergence of the denominator, whereas the numerator remains finite and is not likely to show anomalies near the critical point. Equation 8 indicates that membranes consisting of nonideal lipid mixtures may become mechanically instable toward curvature fluctuations in the neighborhood of the critical mixing/demixing point.

In all measurements of curvature/bending resistance relations, the bending stiffness decreased monotonously with increasing curvature and no discontinuous transitions were observed. We thus conclude that the finding of curvature-induced sorting in ternary lipid mixtures is not associated with an abrupt, first-order phase transition. This hypothesis is supported by the fact that we have not observed any sharp boundaries, which would separate a membrane tube phase from a second phase of the quasiflat (vesicle) reservoir. Accordingly, the composition change as a function of curvature must be a continuous transition toward a phase with a more disordered-phase character, associated with a composition of the tube membrane that does not enter the coexistence region.

In characteristically different regions of the phase diagram than those investigated in this study, in the strong segregation limit far from the critical point, we have, however, observed curvature-dependent nucleation of domains in initially homogeneous phase membrane tubes (not shown). After nucleation, exclusively, a single liquid-disordered domain, with sharp phase boundaries, extended with characteristic square-root growth kinetics that are strongly dependent on curvature. This phenomenon thus shows rather different behavior compared to the measurements described above for the weak segregation limit in the critical neighborhood. A detailed description of these curvature-induced first-order transitions along with an initial theoretical analysis will be the topic of a forthcoming article.

CONCLUSIONS

Our results indicate that curvature-induced lateral lipid segregation in membranes with curvature gradients is amplified in nonideal lipid mixtures. Entropic penalties to sorting that dominate (5) the distribution of ideally diluted trace components, and that also dominate in ideal lipid mixtures,

can thus be overcome by enthalpic contributions from preferential lipid/lipid interactions. The resistance to sorting, expressed in Eqs. 5–8, vanishes at the spinodal line of the ternary mixture phase diagram, where sorting thus becomes maximally efficient.

We note that the phenomenon of curvature-induced demixing that we show here seems to be confirmed by recent independent measurements of pulling forces for tubes extracted from vesicles composed of a multicomponent mixture of several different sphingomyelins plus DOPC and cholesterol (18). Our choice of technique yields the tube radius, and thus does not require the use of reference curvatures.

The measurements described in this report have focused on simple model membrane mixtures. Recent contributions have reported phase transitions (67) and near-critical behavior (68) in vesicles obtained from cellular membranes, indicating strongly nonideal mixing. This suggests that curvature-modulated lateral sorting may be a relevant mechanism for sorting in biological membranes. Trace components, such as DiI dyes (3), have been shown to sort differentially among intracellular biological membranes (3). Our findings suggest that membrane trace components are sorted by sensing the curvature-dependent membrane bulk composition. This sorting mechanism is different from trace components directly sensing membrane curvature, a scenario that we (5), and others (27,69), have found to be inefficient.

Lipid model membrane systems bear the potential for providing further insight into the biophysical contribution of membrane curvature to biological sorting phenomena.

APPENDIX A: SORTING BY SPONTANEOUS CURVATURE

To obtain a relation between the curvature C and the sorting effect $\Delta\varphi_\alpha = \varphi_\alpha(C) - \varphi_{\alpha 0}$, where $\phi_{\alpha 0}$ is the composition of a flat reservoir, we expand the quantity $\overline{\mu}$ about the flat state ($C = 0$),

$$\overline{\mu} = \overline{\mu}_0 + \left(\frac{\partial\overline{\mu}}{\partial C}\right)_0 C + \left(\frac{\partial\overline{\mu}}{\partial\varphi_\alpha}\right)_0 \Delta\varphi_\alpha, \quad (11)$$

where the index 0 indicates that partial derivatives are evaluated at the flat state. For the spontaneous curvature model, the second derivative in Eq. 11 is a function of the spontaneous curvature of the membrane. Equation 5 is obtained from considering diffusional equilibrium $\overline{\mu}(C) = \overline{\mu}_0$ of a flat reservoir (approximated by the vesicle) and bent membrane (tube). Equation 5 can be used to calculate the degree of sorting with specific models, such as the one proposed by Markin (19) and Kozlov and Helfrich (21), who consider an overall spontaneous curvature C_s and bending energy F^{bend} to be a function of composition,

$$C_s(\varphi) = C_\alpha\varphi_\alpha + C_\beta\varphi_\beta$$
$$F^{bend} = \frac{1}{2}\kappa(C - C_s(\varphi))^2 A, \quad (12)$$

where C_i values are molecular spontaneous curvatures of molecule i. From these equations, the following chemical potential can be calculated (for the outer monolayer and molecule α (5)) as

$$\mu_\alpha = a\kappa(C - C_s(\varphi))\varphi_\beta(C_\beta - C_\alpha) + k_BT\ln\varphi_\alpha, \quad (13)$$

where $a = 1/\rho$ is the area per molecule, and k_B is Boltzmann's constant, such that Eq. 5 becomes

$$\Delta\varphi_\alpha = -\left\{\left(\frac{\partial\overline{\mu}}{\partial C}\right)_0 \Big/ \left(\frac{\partial\overline{\mu}}{\partial\varphi_\alpha}\right)_0\right\}C$$
$$= \frac{C}{(C_\alpha - C_\beta) + \frac{k_BT}{a\kappa_0(C_\alpha - C_\beta)}\left(\frac{1}{\varphi_\alpha} + \frac{1}{\varphi_\beta}\right)}. \quad (14)$$

This expression shows that at zero temperature, the curvature C is equal to the difference of spontaneous curvature in the bent and in the flat state,

$$C = C_{s,tube} - C_{s0},$$

and that sorting becomes less efficient at higher temperatures. Using the quantity $\overline{\mu}$, the free energy change of the tube/flat reservoir combination associated with a process at constant area A, is given to second-order by (21)

$$\Delta F = \frac{1}{2}\kappa_0 C^2 A + \frac{1}{2}N\left(\frac{\partial\overline{\mu}}{\partial\varphi_\alpha}\right)_0 \Delta\varphi_\alpha^2 + N\left(\frac{\partial\overline{\mu}}{\partial C}\right)_0 \Delta\varphi_\alpha C. \quad (15)$$

Insertion of Eq. 14 leads to the simple form

$$\Delta F = \frac{1}{2}\kappa_{eff}C^2 A, \quad (16)$$

where the effective bending stiffness is expressed as

$$\kappa_{eff} = \kappa_0 - \rho\left(\frac{\partial\overline{\mu}}{\partial C}\right)_0^2 \Big/ \left(\frac{\partial\overline{\mu}}{\partial\varphi_\alpha}\right)_0$$
$$= \kappa_0 - \frac{a\kappa_0^2(C_\alpha - C_\beta)^2}{a\kappa_0(C_\alpha - C_\beta)^2 + k_BT\left(\frac{1}{\varphi_\alpha} + \frac{1}{\varphi_\beta}\right)}. \quad (17)$$

The effective bending stiffness is thus equivalent to the bare bending stiffness κ_0 if both spontaneous curvatures are equal, or if the temperature is high. An equation equivalent to Eq. 17 has been derived in Kozlov and Helfrich (21) for the case of compressible membranes.

APPENDIX B: SORTING BY BENDING STIFFNESS

For a model that considers a composition-dependent bending stiffness, we have to carry the Taylor expansion of the free energy change comparing flat and bent state up to third-order. A third-order Taylor expansion of F, say in the parameters C and ϕ_i, will in general include homogeneous third-order derivatives such as F_{CCC} and $F_{\varphi_i\varphi_i\varphi_i}$, as well as mixed derivatives and their permutations. For these third-order derivatives, we only consider the terms of $F_{CC\varphi_i}$ of which there are three permutations. Note that we therefore have neglected terms of $F_{\varphi_i\varphi_i\varphi_i}$, i.e., third-order contributions to an order parameter expansion of F, which may not always be justified (70), as Fig. 3 shows. The terms of $F_{CC\varphi_i}$ quantify the composition dependence of the bending stiffness, since κ is defined as

$$\kappa_0 = \frac{1}{A}F_{CC} = \frac{1}{A}\left(\frac{\partial^2 F}{\partial C^2}\right)_0. \quad (18)$$

This definition leads to a relation connecting the third-order derivatives,

$$\left(\partial^2\overline{\mu}/\partial C^2\right) = A/N(\partial\kappa/\partial\varphi_\alpha),$$

and that thus represents two permutations of $F_{CC\varphi_i}$. We thus have, for second- and third-order contributions to the Taylor expansion of the free energy that results from Eq. 3, after inserting intensive parameters expanded to second order, followed by integration (21),

$$\Delta F = \frac{1}{2}\kappa_0 C^2 A + \frac{1}{2}\rho\left(\frac{\partial\overline{\mu}}{\partial\varphi_\alpha}\right)_0 \Delta\varphi_\alpha^2 A + \frac{1}{2}\left(\frac{\partial\kappa}{\partial\varphi_\alpha}\right)_0 \Delta\varphi_\alpha C^2 A. \tag{19}$$

Equation 19 is written to obtain, as required at constant curvature, a first-order homogeneous function in $A = 2\pi R_t L$, where L is the length of the tube. We note that this free energy expansion does not contain contributions from line tension (10,46,71–73), as we did not observe curvature-induced phase transitions with the mixtures examined in this contribution. A free energy functional similar to Eq. 19 has also been considered in Sorre et al. (18). To obtain a relation between composition change and curvature, the expansion of Eq. 11 carried to second-order leads to

$$C^2 = -2\left\{\left(\frac{\partial\overline{\mu}}{\partial\varphi_\alpha}\right)_0 \middle/ \left(\frac{\partial^2\overline{\mu}}{\partial C^2}\right)_0\right\}\Delta\varphi_\alpha$$
$$\quad - \left\{\left(\frac{\partial^2\overline{\mu}}{\partial\varphi_\alpha^2}\right)_0 \middle/ \left(\frac{\partial^2\overline{\mu}}{\partial C^2}\right)_0\right\}\Delta\varphi_\alpha^2, \tag{20}$$

after consideration of diffusional equilibrium and realizing that the first partial derivative term in Eq. 11 is zero for membranes where sorting occurs by bending stiffness only. Equation 20 can be viewed as a second-order series expansion of C^2 in the parameter $\Delta\varphi_\alpha$. Reverting this series (74) yields, to first-order in C^2,

$$\Delta\varphi_\alpha = -\frac{1}{2}\left\{\left(\frac{\partial^2\overline{\mu}}{\partial C^2}\right)_0 \middle/ \left(\frac{\partial\overline{\mu}}{\partial\varphi_\alpha}\right)_0\right\}C^2. \tag{21}$$

Equation 21 is used in Eq. 19 to eliminate the composition dependence. To obtain a mechanical balance equation, Eq. 19 is then amended by the term σA. Minimizing the resulting functional with respect to radius changes at constant tube length results in

$$\sigma = \frac{1}{2}\frac{\kappa_0}{R_t^2} - \frac{3}{8}\left\{\left(\frac{\partial\kappa}{\partial\varphi_\alpha}\right)_0^2 \middle/ \rho\left(\frac{\partial\overline{\mu}}{\partial\varphi_\alpha}\right)_0\right\}\frac{1}{R_t^4} = \frac{1}{2}\frac{\kappa_{\text{eff}}}{R_t^2}, \tag{22}$$

which leads to Eq. 8 of the main text. For the bending stiffness composition-dependence model suggested by Markin (19) and Kozlov and Helfrich (21), we have bending stiffness and energy,

$$\frac{1}{\kappa(\varphi)} = \frac{\varphi_\alpha}{\kappa_\alpha} + \frac{\varphi_\beta}{\kappa_\beta}$$

$$F^{\text{bend}} = \frac{1}{2}\kappa(\varphi)C^2 A, \tag{23}$$

where κ_i values are the molecular bending stiffnesses. These expressions determine the chemical potential for molecule α (5),

$$\mu_\alpha = \frac{1}{2}a\kappa(\varphi)^2 C^2 \varphi_\beta\left(\frac{1}{\kappa_\beta} - \frac{1}{\kappa_\alpha}\right) + k_B T\ln\varphi_\alpha, \tag{24}$$

from which an effective bending stiffness can be obtained as

$$\kappa_{\text{eff}} = \kappa_0 - \frac{3}{4}\left\{\left(\frac{\partial\kappa}{\partial\varphi_\alpha}\right)_0^2 \middle/ \rho\left(\frac{\partial\overline{\mu}}{\partial\varphi_\alpha}\right)_0\right\}C^2$$
$$\quad = \kappa_0 - \frac{3}{4}\frac{a\kappa_0^4\left(\frac{1}{\kappa_\alpha} - \frac{1}{\kappa_\beta}\right)^2}{k_B T\left(\frac{1}{\varphi_\alpha} + \frac{1}{\varphi_\beta}\right)}C^2. \tag{25}$$

As it should, the sorting effect thus disappears if both molecular bending stiffnesses κ_i are equal, as well as if the temperature is large. We have expressed the resistance to sorting in Eqs. 24 and 25 as a mere entropic contribution. In the case of phase-separating mixtures, an interaction term can reduce this resistance to zero at the spinodal line. For these cases, the formalism can easily be generalized to more complex free energy functions that include intermolecular interactions.

SUPPORTING MATERIAL

Supporting materials, methods, and one figure are available at http://www.biophysj.org/biophysj/supplemental/S0006-3495(09)01233-8.

REFERENCES

1. De Matteis, M. A., and A. Luini. 2008. Exiting the Golgi complex. *Nat. Rev. Mol. Cell Biol.* 9:273–284.

2. Holthuis, J. C. M., and T. P. Levine. 2005. Lipid traffic: floppy drives and a superhighway. *Nat. Rev. Mol. Cell Biol.* 6:209–220.

3. Mukherjee, S., T. T. Soe, and F. R. Maxfield. 1999. Endocytic sorting of lipid analogues differing solely in the chemistry of their hydrophobic tails. *J. Cell Biol.* 144:1271–1284.

4. Chinnapen, D. J. F., H. Chinnapen, D. Saslowsky, and W. I. Lencer. 2007. Rafting with cholera toxin: endocytosis and trafficking from plasma membrane to ER. *FEMS Microbiol. Lett.* 266:129–137.

5. Tian, A., and T. Baumgart. 2009. Sorting of lipids and proteins in membrane curvature gradients. *Biophys. J.* 96:2676–2688.

6. Zimmerberg, J., and M. M. Kozlov. 2006. How proteins produce cellular membrane curvature. *Nat. Rev. Mol. Cell Biol.* 7:9–19.

7. McMahon, H. T., and J. L. Gallop. 2005. Membrane curvature and mechanisms of dynamic cell membrane remodeling. *Nature.* 438:590–596.

8. Rustom, A., R. Saffrich, I. Markovic, P. Walther, and H. H. Gerdes. 2004. Nanotubular highways for intercellular organelle transport. *Science.* 303:1007–1010.

9. Simpson, J. C., T. Nilsson, and R. Pepperkok. 2006. Biogenesis of tubular ER-to-Golgi transport intermediates. *Mol. Biol. Cell.* 17:723–737.

10. Baumgart, T., S. T. Hess, and W. W. Webb. 2003. Imaging coexisting fluid domains in biomembrane models coupling curvature and line tension. *Nature.* 425:821–824.

11. Parthasarathy, R., C. H. Yu, and J. T. Groves. 2006. Curvature-modulated phase separation in lipid bilayer membranes. *Langmuir.* 22:5095–5099.

12. Roux, A., D. Cuvelier, P. Nassoy, J. Prost, P. Bassereau, et al. 2005. Role of curvature and phase transition in lipid sorting and fission of membrane tubules. *EMBO J.* 24:1537–1545.

13. Hochmuth, R. M., N. Mohandas, and P. L. Blackshear, Jr. 1973. Measurement of elastic-modulus for red-cell membrane using a fluid mechanical technique. *Biophys. J.* 13:747–762.

14. Bo, L., and R. E. Waugh. 1989. Determination of bilayer-membrane bending stiffness by tether formation from giant, thin-walled vesicles. *Biophys. J.* 55:509–517.

15. Dai, J. W., and M. P. Sheetz. 1998. Cell membrane mechanics. *Methods Cell Biol.* 55:157–171.

16. Allain, J. M., C. Storm, A. Roux, M. B. Amar, and J. F. Joanny. 2004. Fission of a multiphase membrane tube. *Phys. Rev. Lett.* 93:1581041–1581044.

17. Jiang, H. Y., and T. R. Powers. 2008. Curvature-driven lipid sorting in a membrane tubule. *Phys. Rev. Lett.* 101:0181031–0181034.

18. Sorre, B., A. Callan-Jones, J. B. Manneville, P. Nassoy, J. F. Joanny, et al. 2009. Curvature-driven lipid sorting needs proximity to a demixing point and is aided by proteins. *Proc. Natl. Acad. Sci. USA.* 106:5622–5626.

19. Markin, V. S. 1981. Lateral organization of membranes and cell shapes. *Biophys. J.* 36:1–19.

20. Kozlov, M. M., S. L. Leikin, and V. S. Markin. 1989. Elastic properties of interfaces—elasticity moduli and spontaneous geometric characteristics. *J. Chem. Soc., Faraday Trans.* 2(85):277–292.

21. Kozlov, M. M., and W. Helfrich. 1992. Effects of a cosurfactant on the stretching and bending elasticities—a surfactant monolayer. *Langmuir.* 8:2792–2797.

22. Leibler, S. 1986. Curvature instability in membranes. *J. Phys.* 47:507–516.

23. Leibler, S., and D. Andelman. 1987. Ordered and curved meso-structures in membranes and amphiphilic films. *J. Phys.* 48:2013–2018.

24. Seifert, U. 1993. Curvature-induced lateral phase separation in two-component vesicles. *Phys. Rev. Lett.* 70:1335–1338.

25. Bozic, B., V. Kralj-Iglic, and S. Svetina. 2006. Coupling between vesicle shape and lateral distribution of mobile membrane inclusions. *Phys. Rev. E.* 73:0419151.

26. Mukhopadhyay, R., K. C. Huang, and N. S. Wingreen. 2008. Lipid localization in bacterial cells through curvature-mediated microphase separation. *Biophys. J.* 95:1034–1049.

27. Derganc, J. 2007. Curvature-driven lateral segregation of membrane constituents in Golgi cisternae. *Phys. Biol.* 4:317–324.

28. Harden, J. L., and F. C. MacKintosh. 1994. Shape transformations of domains in mixed-fluid films and bilayer-membranes. *Europhys. Lett.* 28:495–500.

29. Harden, J. L., F. C. MacKintosh, and P. D. Olmsted. 2005. Budding and domain shape transformations in mixed lipid films and bilayer membranes. *Phys. Rev. E.* 72:0119031.

30. Julicher, F., and R. Lipowsky. 1993. Domain-induced budding of vesicles. *Phys. Rev. Lett.* 70:2964–2967.

31. Julicher, F., and R. Lipowsky. 1996. Shape transformations of vesicles with intramembrane domains. *Phys. Rev. E.* 53:2670–2683.

32. Kawakatsu, T., D. Andelman, K. Kawasaki, and T. Taniguchi. 1993. Phase transitions and shapes of two-component membranes and vesicles. I. Strong segregation limit. *J. Phys. II (Fr.).* 3:971–997.

33. Taniguchi, T. 1996. Shape deformations and phase separation dynamics of two-component vesicles. *Phys. Rev. Lett.* 76:4444–4447.

34. Baumgart, T., S. Das, W. W. Webb, and J. T. Jenkins. 2005. Membrane elasticity in giant vesicles with fluid phase coexistence. *Biophys. J.* 89:1067–1080.

35. Gozdz, W. T., and G. Gompper. 2001. Shape transformations of two-component membranes under weak tension. *Europhys. Lett.* 55:587–593.

36. Taniguchi, T., K. Kawasaki, D. Andelman, and T. Kawakatsu. 1994. Phase transitions and shapes of two component membranes and vesicles. II. Weak segregation limit. *J. Phys. II (Fr.).* 4:1333–1362.

37. Veksler, A., and N. S. Gov. 2007. Phase transitions of the coupled membrane-cytoskeleton modify cellular shape. *Biophys. J.* 93:3798–3810.

38. Safinya, C. R., E. B. Sirota, D. Roux, and G. S. Smith. 1989. Universality in interacting membranes—the effect of cosurfactants on the interfacial rigidity. *Phys. Rev. Lett.* 62:1134–1137.

39. Dimeglio, J. M., M. Dvolaitzky, and C. Taupin. 1985. Determination of the rigidity constant of the amphiphilic film in birefringent microemulsions—the role of the cosurfactant. *J. Phys. Chem.* 89:871–874.

40. Henriksen, J., A. C. Rowat, and J. H. Ipsen. 2004. Vesicle fluctuation analysis of the effects of sterols on membrane bending rigidity. *Eur. Biophys. J. Biophys. Lett.* 33:732–741.

41. Meleard, P., C. Gerbeaud, T. Pott, L. Fernandez-Puente, I. Bivas, et al. 1997. Bending elasticities of model membranes: influences of temperature and sterol content. *Biophys. J.* 72:2616–2629.

42. Pan, J. J., T. T. Mills, S. Tristram-Nagle, and J. F. Nagle. 2008. Cholesterol perturbs lipid bilayers nonuniversally. *Phys. Rev. Lett.* 100:1981031–1981034.

43. Waugh, R., and E. A. Evans. 1979. Thermoelasticity of red blood-cell membrane. *Biophys. J.* 26:115–131.

44. Hochmuth, R. M., H. C. Wiles, E. A. Evans, and J. T. McCown. 1982. Extensional flow of erythrocyte-membrane from cell body to elastic tether. 2. *Experiment. Biophys. J.* 39:83–89.

45. Hochmuth, R. M., and E. A. Evans. 1982. Extensional flow of erythrocyte-membrane from cell body to elastic tether. 1. *Analysis. Biophys. J.* 39:71–81.

46. Esposito, C., A. Tian, S. Melamed, C. Johnson, S. Y. Tee, et al. 2007. Flicker spectroscopy of thermal lipid bilayer domain boundary fluctuations. *Biophys. J.* 93:3169–3181.

47. Veatch, S. L., and S. L. Keller. 2003. Separation of liquid phases in giant vesicles of ternary mixtures of phospholipids and cholesterol. *Biophys. J.* 85:3074–3083.

48. Veatch, S. L., I. V. Polozov, K. Gawrisch, and S. L. Keller. 2004. Liquid domains in vesicles investigated by NMR and fluorescence microscopy. *Biophys. J.* 86:2910–2922.

49. Griffiths, R. B., and J. C. Wheeler. 1970. Critical points in multicomponent systems. *Phys. Rev. A.* 2:1047–1064.

50. Derenyi, I., F. Julicher, and J. Prost. 2002. Formation and interaction of membrane tubes. *Phys. Rev. Lett.* 88:2381011–2381014.

51. Evans, E., and A. Yeung. 1994. Hidden dynamics in rapid changes of bilayer shape. *Chem. Phys. Lipids.* 73:39–56.

52. Song, J., and R. E. Waugh. 1990. Bilayer-membrane bending stiffness by tether formation from mixed PC-PS lipid vesicles. *J. Biomech. Eng.-Trans. ASME.* 112:235–240.

53. Radhakrishnan, A., and H. McConnell. 2005. Condensed complexes in vesicles containing cholesterol and phospholipids. *Proc. Natl. Acad. Sci. USA.* 102:12662–12666.

54. Harmandaris, V. A., and M. Deserno. 2006. A novel method for measuring the bending rigidity of model lipid membranes by simulating tethers. *J. Chem. Phys.* 125:2049051–2049056.

55. Semrau, S., T. Idema, L. Holtzer, T. Schmidt, and C. Storm. 2008. Accurate determination of elastic parameters for multicomponent membranes. *Phys. Rev. Lett.* 100:0881011–0881014.

56. Rawicz, W., B. A. Smith, T. J. Mclntosh, S. A. Simon, and E. Evans. 2008. Elasticity, strength, and water permeability of bilayers that contain raft microdomain-forming lipids. *Biophys. J.* 94:4725–4736.

57. Rawicz, W., K. Olbrich, T. McIntosh, D. Needham, and E. A. Evans. 2000. Effect of chain length and unsaturation on elasticity of lipid bilayers. *Biophys. J.* 79:328–339.

58. Ly, H. V., D. E. Block, and M. L. Longo. 2002. Interfacial tension effect of ethanol on lipid bilayer rigidity, stability, and area/molecule: a micropipette aspiration approach. *Langmuir.* 18:8988–8995.

59. Marsh, D. 2006. Elastic curvature constants of lipid monolayers and bilayers. *Chem. Phys. Lipids.* 144:146–159.

60. Henriksen, J. R., and J. H. Ipsen. 2004. Measurement of membrane elasticity by micropipette aspiration. *Eur. Phys. J. E.* 14:149–167.

61. Leung, S., and R. Griffiths. 1973. Thermodynamic properties near liquid-vapor critical line in mixtures of He-3 and He-4. *Phys. Rev. A.* 8:2670–2683.

62. Anisimov, M. A., and J. V. Sengers. 1992. On the choice of a hidden field variable near the critical-point of fluid mixtures. *Phys. Lett. A.* 172:114–118.

63. Chu, N., N. Kucerka, Y. F. Liu, S. Tristram-Nagle, and J. F. Nagle. 2005. Anomalous swelling of lipid bilayer stacks is caused by softening of the bending modulus. *Phys. Rev. E.* 71:0419041–0419047.

64. Mecke, K. R., T. Charitat, and F. Graner. 2003. Fluctuating lipid bilayer in an arbitrary potential: theory and experimental determination of bending rigidity. *Langmuir*. 19:2080–2087.

65. Dimova, R., B. Pouligny, and C. Dietrich. 2000. Pretransitional effects in dimyristoylphosphatidylcholine vesicle membranes: optical dynamometry study. *Biophys. J*. 79:340–356.

66. Evans, E., and R. Kwok. 1982. Mechanical calorimetry of large dimyristoylphosphatidylcholine vesicles in the phase-transition region. *Biochemistry*. 21:4874–4879.

67. Baumgart, T., A. T. Hammond, P. Sengupta, S. T. Hess, D. Holowka, et al. 2007. Large scale fluid/fluid phase separation of proteins and lipids in giant plasma membrane vesicles. *Proc. Natl. Acad. Sci. USA*. 104:3165–3170.

68. Veatch, S. L., P. Cicuta, P. Sengupta, A. Honerkamp-Smith, D. Holowka, et al. 2008. Critical fluctuations in plasma membrane vesicles. *ACS Chem. Biol*. 3:287–293.

69. Cooke, I. R., and M. Deserno. 2006. Coupling between lipid shape and membrane curvature. *Biophys. J*. 91:487–495.

70. Chaikin, P., and T. Lubensky. 1995. Principles of Condensed Matter Physics. Cambridge University Press, Cambridge, UK.

71. Tian, A., C. Johnson, W. Wang, and T. Baumgart. 2007. Line tension at fluid membrane domain boundaries measured by micropipette aspiration. *Phys. Rev. Lett*. 98:2081021–2081024.

72. Heinrich, M., I. Levental, H. Gelman, P. Janmey, and T. Baumgart. 2008. Critical exponents for line tension and dipole density difference from lipid monolayer domain boundary fluctuations. *J. Phys. Chem. B*. 112:8063–8068.

73. Honerkamp-Smith, A. R., P. Cicuta, M. D. Collins, S. L. Veatch, M. den Nijs, et al. 2008. Line tensions, correlation lengths, and critical exponents in lipid membranes near critical points. *Biophys. J*. 95:236–246.

74. McQuarrie, D. 2000. Statistical Mechanics. University Science Books, Sausalito, CA.